Journal of Molecular Graphics and Modelling 28 (2010) 863–869

Contents lists available at ScienceDirect

Journal of Molecular Graphics and Modelling

journal homepage: www.elsevier.com/locate/JMGM

Molecular dynamics simulation of the effect of ligand homogeneity on protein behavior in hydrophobic charge induction chromatography

Lin Zhang, Shu Bai, Yan Sun*

Department of Biochemical Engineering, School of Chemical Engineering and Technology, Tianjin University, Tianjin 300072, China

ARTICLE INFO

Article history:
Received 15 December 2009
Received in revised form 7 March 2010
Accepted 14 March 2010
Available online 23 March 2010

Keywords:
Protein chromatography
Adsorption
Elution
Irreversibility
Protein unfolding
Molecular dynamics

ABSTRACT

Hydrophobic charge induction chromatography (HCIC) is an adsorption chromatography combining hydrophobic interaction in adsorption with electrostatic repulsion in elution. Ligand density has significant effects on protein adsorption behavior, but little is understood about the effect of ligand homogeneity on surface morphology of ligands, protein conformational transition and dynamics within adsorbent pore due to the lack of microscopic experimental techniques. In the present study, a coarse-grained adsorbent pore model established in an earlier work is used to represent the actual porous adsorbent composed of matrix and immobilized HCIC ligands. Two adsorbent pores with different ligand distributions are constructed by adjusting the coupling sites, denoted as L1 and L2. In L1 the ligands are bonded uniformly while in L2 the ligands are arranged in lines in the axial direction and thus exhibit a heterogeneous distribution. Protein adsorption, desorption, and conformational transition in both L1 and L2 are shown by molecular dynamics simulations of a 46-bead β-barrel coarse-grained model protein within the adsorbent pore models. The simulations indicate that ligand homogeneity has significant effect on both the irreversibility and the dynamics of adsorption while no obvious effect on protein conformation distribution. In comparison with L1, L2 leads to irreversible and slow adsorption, indicating the strict requirement of a suitable protein orientation to reach stable adsorption. The simulations have provided new insight into the microscopic behavior of HCIC, which would be beneficial to the rational design of adsorbents and parameter optimization for high-performance HCIC.

1. Introduction

Separation and purification are the key steps for the production of proteins expressed by recombinant DNA technology [1,2], and chromatographic methods play the central role in the downstream processes. Of the various chromatographic methods based on the different interactions between ligands and proteins, hydrophobic charge induction chromatography (HCIC) is an adsorption chromatography combining hydrophobic interaction in adsorption with electrostatic repulsion in elution [3,4]. An HCIC adsorbent is coupled with a hydrophobic ligand with a weak base or acid group, which is not charged at neutral pH range. Therefore, at physiological conditions, no charge is carried in the ligand, and protein adsorption occurs through protein–ligand hydrophobic interaction. When the pH of the mobile phase is reduced below the pK_a of the basic ligand as well as the isoelectric point of protein, both the protein and ligand carry positive charges and dissociation occurs on the basis of protein–ligand electrostatic repulsion. Thus, HCIC is advantageous of its ease of bound protein elution. Consequently, HCIC adsorbents can be made at very high ligand densities to achieve high adsorption capacity with little difficulty in the elution of bound proteins. To date, it has been applied in the separation and purification of antibodies [3,5–10] and various other proteins [7,11–14].

Various experimental studies have been performed on the macroscopic behaviors in HCIC, including the optimization of operational parameters [3,13], examination of adsorption behavior and construction of theoretical models [15–18], and screening of ligands [12]. Ligand distribution, homogeneous or heterogeneous, is considered to affect protein adsorption behavior [19], but little is understood about this effect on surface morphology of ligands, protein conformational transition and dynamics within adsorbent pores due to the lack of powerful microscopic experimental techniques.

In an earlier work [20], the authors have constructed a coarse-grained adsorbent pore model to represent the actual porous adsorbent composed of the matrix and immobilized HCIC ligands, and provided molecular insight into protein conformational transition within adsorbent pores using molecular dynamics simulations. In the present study, the adsorbent pore model is modified to investigate the effect of ligand distribution. Adsorbent pores with two different ligand distributions are constructed by adjusting the coupling sites, denoted as L1 and L2. In L1 the ligands are bonded

* Corresponding author. Tel.: +86 22 27404981; fax: +86 22 27406590.
E-mail address: ysun@tju.edu.cn (Y. Sun).

1093-3263/$ – see front matter © 2010 Elsevier Inc. All rights reserved.
doi:10.1016/j.jmgm.2010.03.006

Nomenclature

B	stably adsorbed state of protein
d	the minimum distance between the protein and ligands
D	desorbed state of protein
E	inter-molecular interaction energy between protein and ligands
f	mole fraction
L1	adsorbent pore with uniform ligand distribution
L2	adsorbent pore with heterogeneous ligand distribution
M	intermediate state of protein
M_T	total number of trajectories
N	native state of protein
R_g	radius of gyration of protein
U	unfolded state of protein
Y_B	adsorption irreversibility
Y_D	Desorption irreversibility
χ	structural overlap function

uniformly while in L2 the ligands are arranged in lines in the axial pore direction. Thus L1 and L2 are employed to represent a homogeneous ligand distribution and a heterogeneous one, respectively. In both L1 and L2, the protein adsorption and desorption behaviors, as well as its conformational transition are monitored by molecular dynamics simulations using a 46-bead β-barrel coarse-grained model protein within the pores. The effect of ligand distribution is explored with an emphasis on the microscopic process.

2. Models and methods

2.1. Protein model

In the present study, a 46-bead β-barrel coarse-grained model protein [21] is used. It consists of 46 amino acid residues in the sequence $H_9N_3(PH)_4N_3H_9N_3(PH)_5P$, where H, P, and N represents hydrophobic, hydrophilic and neutral residues, respectively. In this simplified model, all residues are treated as spherical beads of equal size, connected by covalent bonds. The bond length is 0.38 nm. The potential function has been well-defined for protein folding/unfolding [21]. Using simulated annealing method, the native structure of the model protein is obtained, as shown in Fig. S1a. The effect of temperature has also been examined [22,23]. The temperature dependence of refolding has been provided to evaluate the refolding behavior of the model protein [24]. This has been repeated in our simulation results (data not shown). In the present study, a temperature in the transition region between the folded state and unfolded state, 298.15 K, is used to study the conformational transition. It can be seen that this model protein has both the hydrophobic core and exposed hydrophilic residues on the surface, and its refolding is driven by intramolecular hydrophobic interaction, which are general to protein molecules. Therefore, this protein model has been extensively used to simulate actual protein molecules in molecular simulations of protein folding [22,23] and aggregation [25,26]. A charged state of the model protein is also defined as described in an earlier work [20,27] to simulate the protein in desorption, where all hydrophilic beads carry net charge and are thus included in the calculation of Coulomb potential energy (Table S1). It is verified by simulated annealing that the model protein retains its native structure in the charged state but has a flatter structure (data not shown). Details of the model protein are described in Supporting Information.

2.2. HCIC adsorbent pore model

In the present study, the coarse-grained ligand model consists of two hydrophobic beads, H1, H2 and a hydrophobic chargeable bead, HQ at the end. It is constructed to simulate 4-mercaptoethylpyridine (MEP, pK_a 4.85), as shown in Fig. S1b. Details of the ligand model are described in Supporting Information. The ligands are then immobilized on the interior surface of a cylinder with infinite length to simulate the HCIC adsorbent pore. In the present study, the average ligand density on the pore surface is 2.212 μmol/m^2. The ligand bonding is modified to construct adsorbent pores with two different ligand distributions, denoted as L1

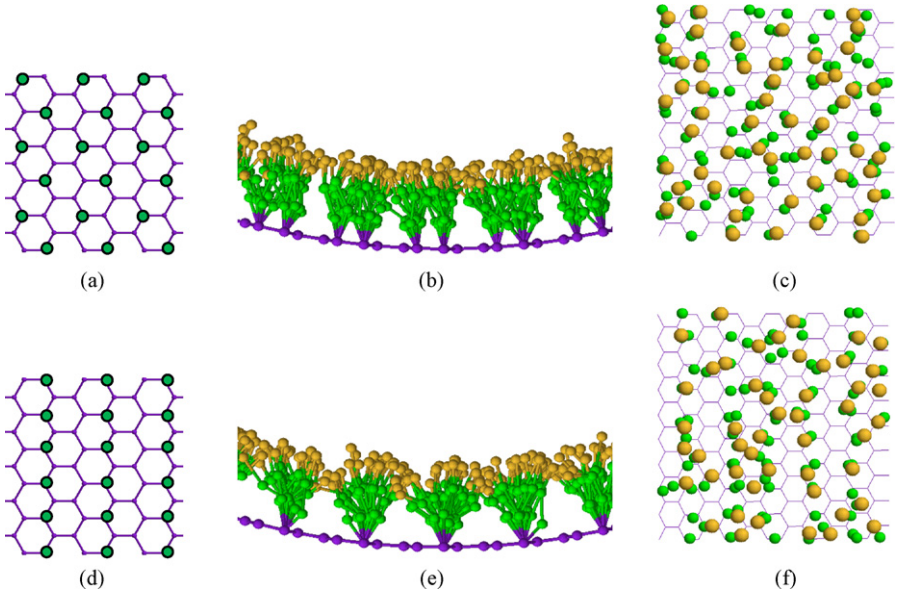

Fig. 1. HCIC adsorbent pore models: the distribution of coupling sites (a), the front view (b) and vertical view (c) of the surface morphology of equilibrated adsorbent pores in L1. The counterparts in L2 are shown in (d–f). The coupling sites are drawn as green dots. Beads H1 and H2 of the ligands are drawn in green while bead HQ is drawn in yellow. The beads in matrix are drawn in purple. Only a part of the adsorbent pore is shown for a clear view: (a) is after our previous work [27]. (For interpretation of the references to color in this figure legend, the reader is referred to the web version of the article.)

and L2, by adjusting the coupling sites. In L1 the ligands are bonded uniformly (Fig. 1a). The smallest distance between neighboring ligands is 2.0 nm, followed by 2.646 and 3.0 nm. Therefore, a narrow distance distribution is observed and a homogeneous ligand surface is obtained, where the matrix is shown in purple and the coupling sites are shown in green dots. In L2 the ligands are arranged in lines in the axial direction (Fig. 1d). The smallest distance between neighboring ligands is 1.732 nm, followed by 3.0 and 3.464 nm. In comparison with L1, the distance distribution is much wider, that is, the distance fluctuates intensively, indicating a non-homogeneous distribution of coupling sites and thus a heterogeneous ligand surface.

2.3. Simulation methods

The Langevin dynamics and NVT ensemble are used to examine the conformational transition of the model protein within the HCIC adsorbent pore, using GROMACS 3.3.3 [28,29] as the platform and the procedure proposed in the previous work [20]. Twenty-five independent simulations are performed for each set of conditions. All snapshots are prepared using the Rasmol program [30].

Protein conformation is quantitatively distinguished by two parameters: the protein's radius of gyration (R_g) and the structural overlap function (χ), as described in the previous studies [31,32]. The native (N), intermediate (M), and unfolded (U) states are defined by Formula S4. The molar fraction is denoted as f. For instance, f_U is the fraction of unfolded state. To examine the adsorption behavior of the protein, the stable adsorbed state (B) and desorbed state (D) are defined by Formula S5. Then, a parameter Y_B is defined by Formula S6 to evaluate the adsorption irreversibility. Once adsorbed, the protein may remain at the adsorbed state until the simulation end, which is a case of $Y_B = 1$. Thus, $Y_B = 1$ indicates complete irreversible adsorption. The protein may also be stripped from the ligand surface, which is a case of $Y_B < 1$. Therefore, more desorption causes smaller Y_B. That is, smaller Y_B indicates more reversible tendency of the adsorption.

More details of this simulation are given in Supporting Information.

3. Results and discussion

3.1. Surface morphology of ligands

The equilibrated conformation of ligands is examined through a 100 ns MD simulation in the empty adsorbent pore, i.e., without protein, as shown in Fig. 1. The ligand distribution is varied as L1 (Fig. 1a) and L2 (Fig. 1d).

As can be seen in Fig. 1b, after the pre-equilibration stage, though the beads H1 and H2 at the head of ligand have a heterogeneous distribution due to the restriction from the coupling sites, bead HQ at the tail of ligand has a uniform distribution, leading to a homogeneous ligand surface in L1, in which the matrix surface is covered by the ligand (Fig. 1c). In L2, the coupling sites have a line-shaped arrangement in the axial direction (Fig. 1d). Therefore, bead HQ at the end of ligand swings around the coupling site, leading to a wave-shaped distribution (Fig. 1e). That is, more regions on matrix are exposed to the mobile phase in comparison with L1, leading to a heterogeneous ligand surface (Fig. 1f).

3.2. Adsorption

To examine the adsorption process, a native protein is randomly placed into the equilibrated adsorbent pore for a 100 ns simulation. Two pores, L1 and L2, are used to investigate the effect of ligand distribution. The dynamic trajectories in L1 are shown in Fig. 2a, including the time courses of χ, R_g, d and E, in which the first two

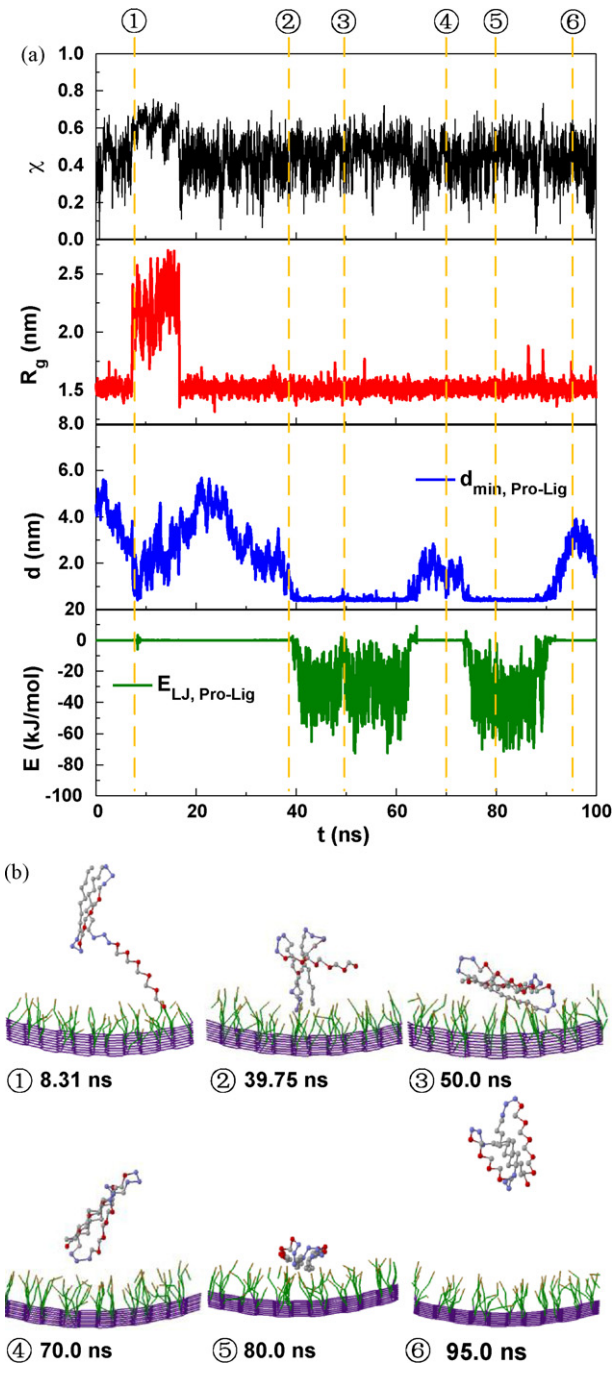

Fig. 2. Adsorption behavior in L1. The time courses of χ, R_g, d and E in adsorption trajectory are shown in (a), and the corresponding snapshots at the time points marked in (a) are shown in (b).

parameters refer to the protein conformation and the other two refer to the protein–ligand interactions. The representative time points in these trajectories are marked and the corresponding snapshots are shown in Fig. 2b. The counterparts for L2 are shown in Fig. 3a and b.

In L1 (Fig. 2a), unfolding is observed (as indicated by the high values of χ and R_g) when the protein approaches the ligands at 8.31 ns (indicated by low d). The snapshot at this time point (snapshot No. 1 in Fig. 2b) shows that a chain of the protein extends toward the ligands and makes a transitory contact. However, this contact is unfavorable because the hydrophilic beads (red) are repulsed by the hydrophobic ligands. This corresponds to the positive LJ

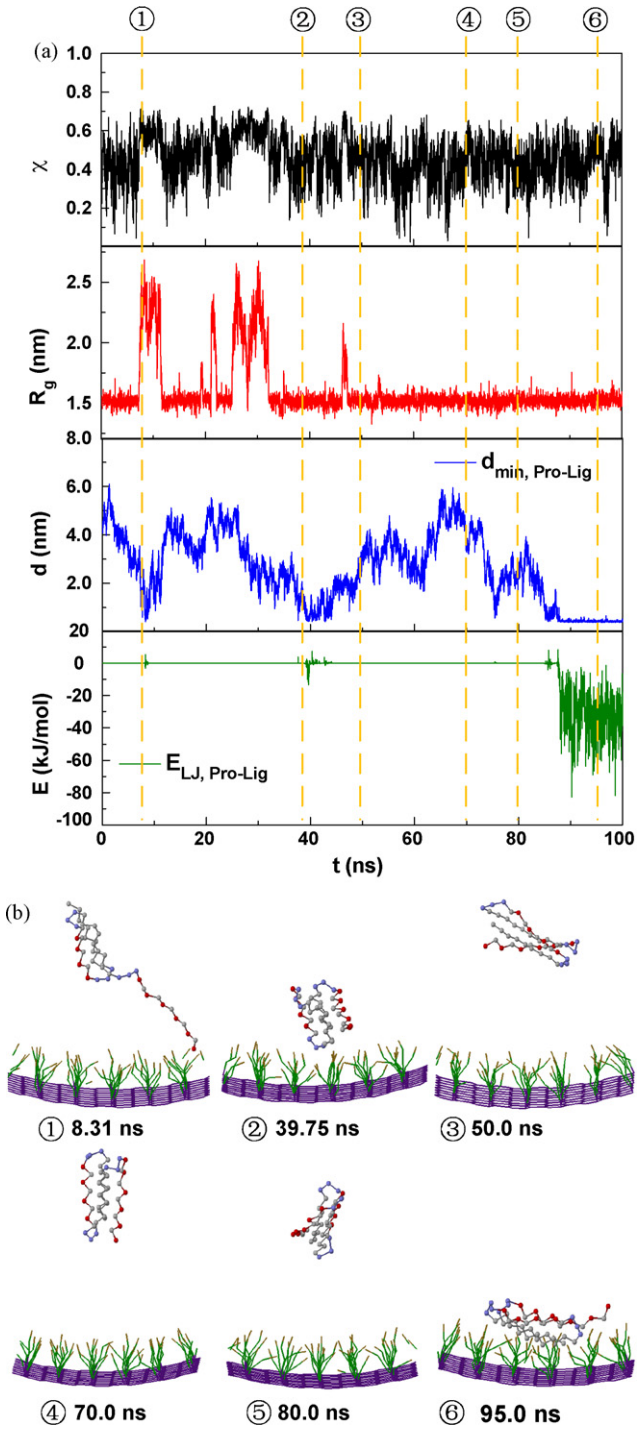

Fig. 3. Adsorption behavior in L2. The time courses of χ, R_g, d and E in adsorption trajectory are shown in (a), and the corresponding snapshots at the time points marked in (a) are shown in (b).

potential energy observed at this time point (E). Thus, the protein moves away from the ligands, indicated by the increase of d. In this process, the protein can get refolded due to the intramolecular hydrophobic interaction (see the changes in χ and R_g), and the adjustment of protein orientation is also observed. At 39.75 ns, the protein approaches the ligands again. Here, the hydrophilic beads in the protein are always repulsed while the hydrophobic beads are always attracted due to the homogeneous hydrophobic ligand surface, leading to a disturbance of protein conformation (see snapshot No. 2 in Fig. 2b). Then, stable adsorption is observed, indicated by the steady low value of d and negative LJ potential energy. The snapshot at 50.0 ns is a representative stably adsorbed conformation, where the hydrophobic chain is stably adsorbed in a parallel orientation and two chains containing hydrophilic beads are repulsed away from the ligands. At 70.0 ns, the protein leaves the surface but keeps at the neighborhood of ligands. After a small adjustment of protein orientation, adsorption occurs once again at 80.0 ns with a perfect orientation. However, desorption is observed again at 95.0 ns. The results imply that the protein adsorption in L1 is reversible.

Table 1
The irreversibility parameter in adsorption and desorption processes.

Adsorbent	Adsorption, Y_B	Desorption, Y_D
L1	0.786 (0.204[a])	0.929 (0.085)
L2	0.937 (0.117)	0.963 (0.051)

[a] The number in the parentheses indicates the standard deviation of 25 independent simulations.

In L2 (Fig. 3a), similar protein adsorption and conformation transition are observed as in L1 at the initial stage. At 8.31 ns, the protein unfolds and makes a transitory contact (see Fig. 3b). At 39.75 ns, the protein approaches the ligands again. Here, remarkable differences in these two ligand distributions are observed. In L2, it is difficult for the protein to reach stable adsorbed state due to the heterogeneous distribution of hydrophobic ligands. Once the protein approaches the ligands in an unfavorable orientation, larger repulsion is observed due to the locally concentrated ligands (Fig. 1c). That is, stricter protein orientation is needed for the protein to get adsorbed. Thus, it can be seen that the protein cannot be adsorbed as in L1 at 39.75 ns, though many tries are observed indicated by the low d (blue). At 50.0 ns, the protein is far away from the ligands, and remains a free state at 70.0 ns. At 80.0 ns, an adjustment of protein orientation is observed, followed finally by a stable adsorption at 95.0 ns with a perfect orientation. Therefore, it is considered that strict protein orientation is necessary for the protein to reach a stable adsorption in L2, so the first passage time is longer than that in L1, indicating slower adsorption.

The above discussion indicates that ligand distribution has a remarkable effect on both the adsorption irreversibility and kinetics. Moreover, Y_B is calculated from the 25 independent simulations for the quantitative analysis of adsorption irreversibility, as shown in Table 1. It can be seen that Y_B in L2 is larger than that in L1, indicating enhanced adsorption irreversibility. The average times (calculated from the 25 trajectories) for the protein to come in contact with the ligand surface are 34.37 and 37.67 ns in L1 and L2, respectively. It can be seen that the time to get adsorption in L2 is larger than that in L1, indicating slower adsorption. These are the further validation for the discussions on the trajectories.

3.3. Desorption

In desorption, the pH in the mobile phase should be reduced below the pK_a of ligands as well as the isoelectric point of protein, when both the protein and ligands carry positive charges and thus the protein is repulsed from the ligand surface. From the end of the adsorption, the charge numbers on the hydrophilic beads in protein and the bead HQ in the ligand are all adjusted to +0.4 to simulate the desorption process. Fig. 4a shows the time courses of χ, R_g, d and E in L1. The snapshots at the time points marked in (a) are shown in Fig. 4b. The counterparts in L2 are shown in Fig. 5.

Fig. 4 shows an obvious difference between the desorption processes in homogeneous and heterogeneous ligand surfaces. In L1, the protein remains on the ligand surface at 0.12 ns, though a chain containing hydrophilic beads is repulsed away from the ligands (Fig. 4b). In this process, simultaneous hydrophobic attraction and

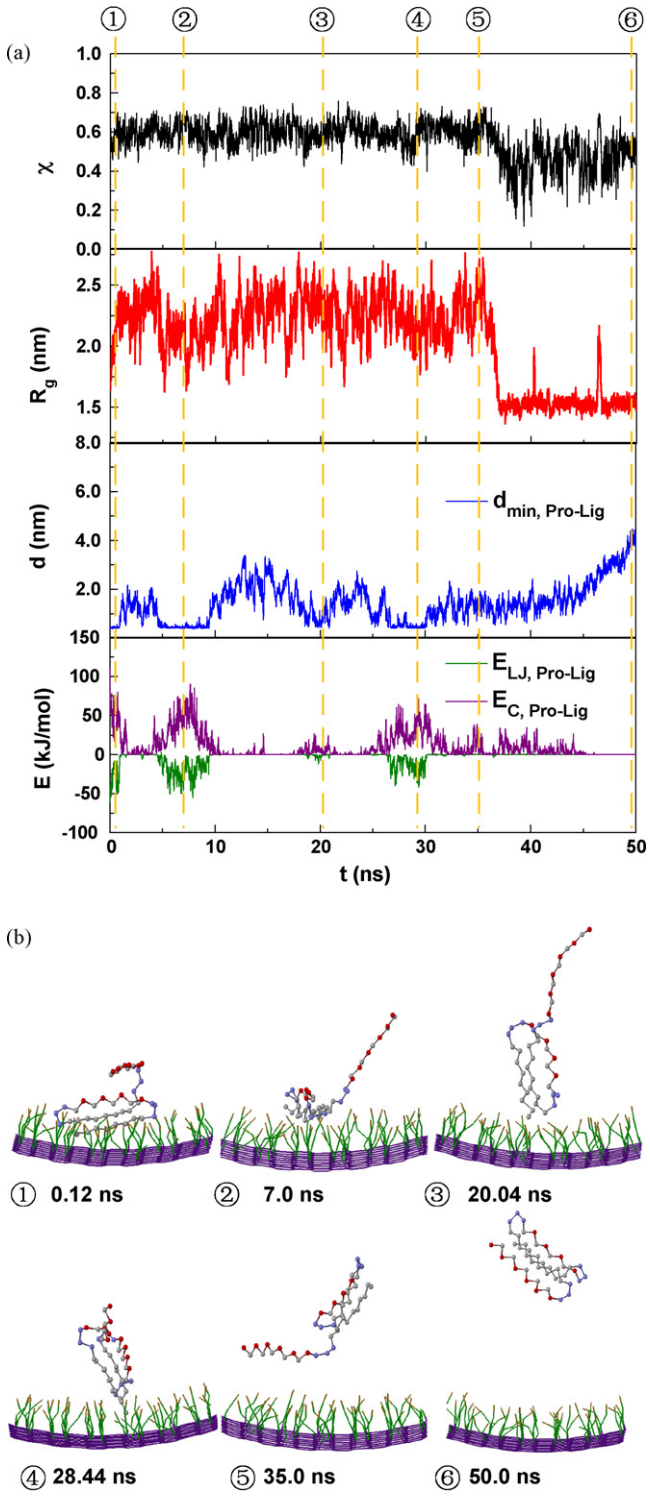

Fig. 4. Desorption behavior in L1. The time courses of χ, R_g, d and E in adsorption trajectory are shown in (a), and the corresponding snapshots at the time points marked in (a) are shown in (b).

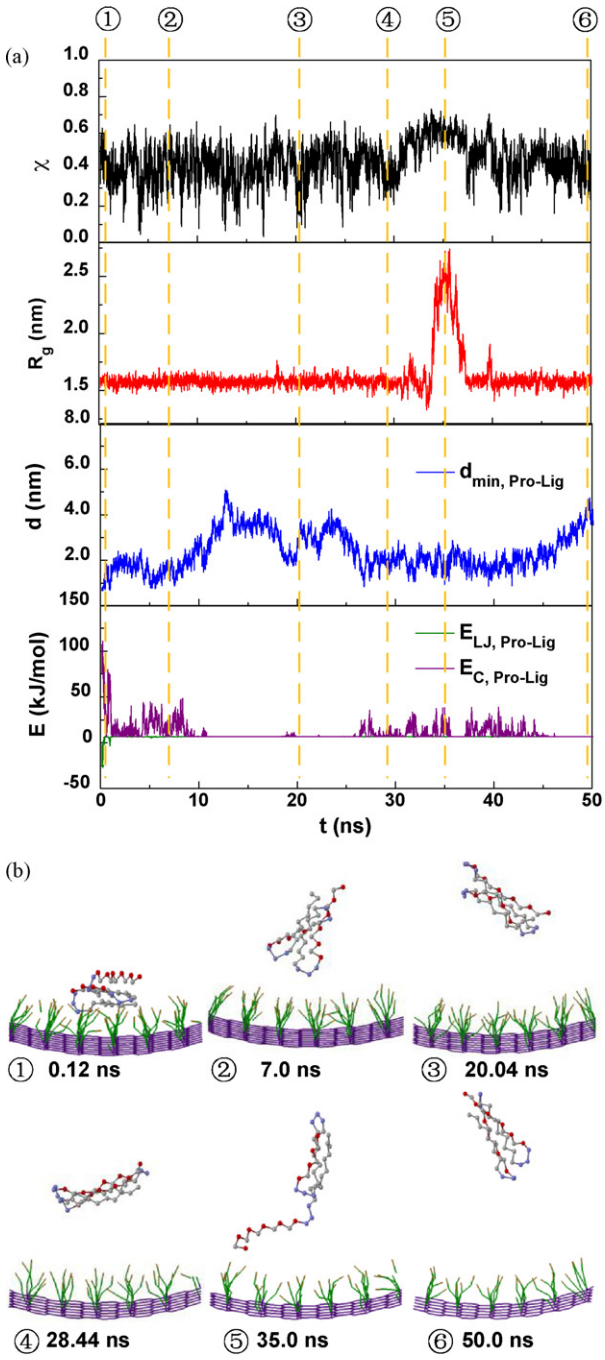

Fig. 5. Desorption behavior in L2. The time courses of χ, R_g, d and E in adsorption trajectory are shown in (a), and the corresponding snapshots at the time points marked in (a) are shown in (b). (For interpretation of the references to color in text, the reader is referred to the web version of the article.)

electrostatic repulsion are observed, indicated by the negative LJ potential energy (green) and positive Coulomb potential energy (purple). Thus, the protein structure is seriously extended, indicated by the continuous high values of χ and R_g. At 0.92 ns, the protein is repulsed, indicated by a large d. Because the ligands are well distributed on the surface, however, hydrophobic attraction on the protein is frequently observed, leading to an adsorption occurred at 4.64 ns, indicated by the continuous low d from 4.64 ns. In the following, several temporary adsorbed states are observed, for instance, at 20.04 and 28.44 ns (Fig. 4b). However, desorbed state is the majority. At the end of simulation, the protein remains a completely desorbed state with native conformation.

In L2, electrostatic repulsion is enhanced due to the locally concentrated ligands in a heterogeneous distribution. Therefore, the protein is readily desorbed and no adsorption is observed again thereafter, indicated by the continuous large d (Fig. 5a, blue). In this process, though the protein approaches the ligands many times, for instance, at 7.0 and 35.0 ns (Fig. 5b), adsorption is prevented by the long-range electrostatic repulsion (Fig. 5a, purple). At the end

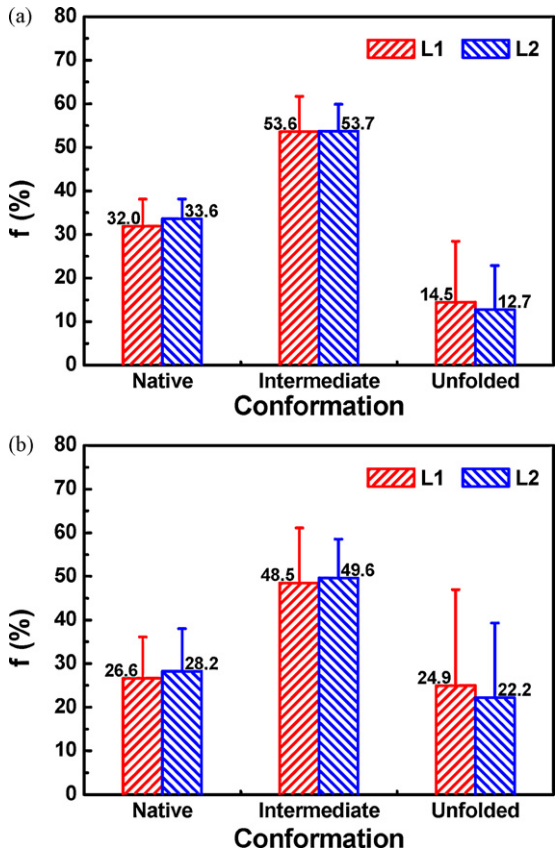

Fig. 6. The protein fractions of different conformation in adsorption (a) and desorption (b). Both L1 and L2 are examined and the exact values are marked in the figure.

of simulation, the protein is in a completely desorbed state with native conformation, similar to that in L1.

Similar with the adsorption process, Y_D is calculated from the 25 independent simulations, to quantitatively examine the effect of ligand distribution on the desorption irreversibility (Table 1). It can be seen that Y_D in L1 is smaller than that in L2, indicating the existence of adsorption–desorption transition in L1. The average times for desorption are also calculated from the 25 trajectories. The values are 2.70 and 1.85 ns in L1 and L2, respectively. It can be seen that the time to get desorption in L2 is smaller than that in L1, indicating faster desorption. These are consistent with the discussions regarding Figs. 4 and 5.

3.4. Protein conformational transition

To examine the effect of ligand distribution on protein conformational transition, the protein fractions of different conformations are calculated from the 25 independent simulations. The results are shown in Fig. 6, in which the exact values are marked.

Fig. 6a shows that in the adsorption process there is no significant difference of protein conformations (including native, intermediate, and unfolded) between the two ligand distributions. In the desorption process (Fig. 6b), however, somewhat larger native fraction and smaller unfolded fraction are observed in L2. This is consistent with the unfolding observed in Fig. 4. Moreover, in both L1 and L2, the unfolded fraction in desorption is remarkably (over twofold) larger than that in adsorption, indicating that the simultaneous hydrophobic attraction and electrostatic repulsion on the protein causes serious protein unfolding in the desorption process.

4. Conclusions

Coarse-grained adsorbent pores with two different ligand distributions, denoted by L1 and L2 are constructed by adjustment of coupling sites. In L1, a homogeneous ligand surface is observed due to the well distributed coupling sites, while in L2, a heterogeneous ligand surface is observed due to the line-shaped arrangement of coupling sites in the axial direction. Molecular dynamics simulations are performed to examine the protein adsorption, desorption and conformational transition within the adsorbent pores, using a 46-bead β-barrel coarse-grained model protein. The simulation results show that ligand bonding has remarkable effect on the irreversibility and dynamics of adsorption. Larger adsorption irreversibility is observed in L2 in comparison with in L1. Moreover, slower adsorption in L2 indicates that the ligands with line-shaped distribution have higher selectivity of protein orientation. That is, protein has to adjust its orientation to match the ligand surface for stable adsorption, leading to a slower rate. Faster desorption in L2 indicates that locally concentrated ligands provide enhanced protein–ligand electrostatic repulsion and speed up the dissociation. Protein conformation distribution shows no obvious difference between L1 and L2. Therefore, homogeneous ligand surface can provide high adsorption rate while heterogeneous ligand surface with line-shaped distribution of coupling sites (match the hydrophobic region on protein surface here) can provide high selectivity on protein conformation and orientation. This should be balanced and optimized according to the target protein. The simulation results have examined the microscopic behavior of HCIC, which would be beneficial to the fabrication and application of adsorbents.

Acknowledgments

This work was supported by the Natural Science Foundation of China (Nos. 20636040 and 20976126) and the China Postdoctoral Science Foundation (No. 20080440679).

Appendix A. Supplementary data

Supplementary data associated with this article can be found, in the online version, at doi:10.1016/j.jmgm.2010.03.006.

References

[1] B. Leader, Q.J. Baca, D.E. Golan, Protein therapeutics: a summary and pharmacological classification, Nat. Rev. Drug Discov. 7 (2008) 21–39.
[2] R. Sodoyer, Expression systems for the production of recombinant pharmaceuticals, Biodrugs 18 (2004) 51–62.
[3] S.C. Burton, D.R. Harding, Hydrophobic charge induction chromatography: salt independent protein adsorption and facile elution with aqueous buffers, J. Chromatogr. A 814 (1998) 71–81.
[4] S.C. Burton, N.W. Haggarty, D.R. Harding, One step purification of chymosin by mixed mode chromatography, Biotechnol. Bioeng. 56 (1997) 45–55.
[5] W. Schwartz, D. Judd, M. Wysocki, L. Guerrier, E. Birck-Wilson, E. Boschetti, Comparison of hydrophobic charge induction chromatography with affinity chromatography on protein A for harvest and purification of antibodies, J. Chromatogr. A 908 (2001) 251–263.
[6] M.P. Dux, R. Barent, J. Sinha, M. Gouthro, T. Swanson, A. Barthuli, M. Inan, J.T. Ross, L.A. Smith, T.J. Smith, R. Webb, B. Loveless, I. Henderson, M.M. Meagher, Purification and scale-up of a recombinant heavy chain fragment C of botulinum neurotoxin serotype E in Pichia pastoris GS115, Protein Expres. Purif. 45 (2006) 359–367.
[7] G.T. Weatherly, A. Bouvier, D.D. Lydiard, J. Chapline, I. Henderson, J.L. Schrimsher, S.R. Shepard, Initial purification of recombinant botulinum neurotoxin fragments for pharmaceutical production using hydrophobic charge induction chromatography, J. Chromatogr. A 952 (2002) 99–110.
[8] L. Guerrier, P. Girot, W. Schwartz, E. Boschetti, New method for the selective capture of antibodies under physiological conditions, Bioseparation 9 (2000) 211–221.
[9] L. Guerrier, I. Flayeux, E. Boschetti, A dual-mode approach to the selective separation of antibodies and their fragments, J. Chromatogr. B 755 (2001) 37–46.
[10] E. Boschetti, Antibody separation by hydrophobic charge induction chromatography, Trends Biotechnol. 20 (2002) 333–337.

[11] G.F. Zhao, Y. Sun, Displacement chromatography of proteins on hydrophobic charge induction adsorbent column, J. Chromatogr. A 1165 (2007) 109–115.
[12] S. Ghose, B. Hubbard, S.M. Cramer, Evaluation and comparison of alternatives to Protein A chromatography—mimetic and hydrophobic charge induction chromatographic stationary phases, J. Chromatogr. A 1122 (2006) 144–152.
[13] D. Coulon, C. Cabanne, V. Fitton, A.M. Noubhani, E. Saint-Christophe, X. Santarelli, Penicillin acylase purification with the aid of hydrophobic charge induction chromatography, J. Chromatogr. B 808 (2004) 111–115.
[14] G.F. Zhao, G.Y. Peng, F.Q. Li, Q.H. Shi, Y. Sun, 5-Aminoindole, a new ligand for hydrophobic charge induction chromatography, J. Chromatogr. A 1211 (2008) 90–98.
[15] D. Gao, D.Q. Lin, S.J. Yao, Patch controlled protein adsorption in mixed-mode chromatography with benzylamine as functional ligand, Biochem. Eng. J. 38 (2008) 355–361.
[16] D. Gao, D.Q. Lin, S.J. Yao, Mechanistic analysis on the effects of salt concentration and pH on protein adsorption onto a mixed-mode adsorbent with cation ligand, J. Chromatogr. B 859 (2007) 16–23.
[17] D. Gao, D.Q. Lin, S.J. Yao, Protein adsorption kinetics of mixed-mode adsorbent with benzylamine as functional ligand, Chem. Eng. Sci. 61 (2006) 7260–7268.
[18] D. Gao, D.Q. Lin, S.J. Yao, Measurement and correlation of protein adsorption with mixed-mode adsorbents taking into account the influences of salt concentration and pH, J. Chem. Eng. Data 51 (2006) 1205–1211.
[19] X. Li, V.L. McGuffin, Theoretical evaluation of methods for extracting retention factors and kinetic rate constants in liquid chromatography, J. Chromatogr. A 1203 (2008) 67–80.
[20] L. Zhang, G.F. Zhao, Y. Sun, Molecular insight into protein conformational transition in hydrophobic charge induction chromatography: a molecular dynamics simulation, J. Phys. Chem. B 113 (2009) 6873–6880.
[21] J.D. Honeycutt, D. Thirumalai, Metastability of the folded states of globular proteins, Proc. Natl. Acad. Sci. U.S.A. 87 (1990) 3526–3529.
[22] T. Veitshans, D. Klimov, D. Thirumalai, Protein folding kinetics: timescales, pathways and energy landscapes in terms of sequence-dependent properties, Fold. Des. 2 (1997) 1–22.
[23] Z. Guo, D. Thirumalai, Folding kinetics of proteins: a model study, J. Chem. Phys. 97 (1992) 525–535.
[24] Z. Guo, D. Thirumalai, Kinetics of protein folding: nucleation mechanism, time scales, and pathways, Biopolymers 36 (1995) 83–102.
[25] T Cellmer, D. Bratko, J.M. Prausnitz, H. Blanch, The competition between protein folding and aggregation: off-lattice minimalist model studies, Biotechnol. Bioeng. 89 (2005) 78–87.
[26] H.B. Jang, C.K. Hall, Y.Q. Zhou, Assembly and kinetic folding pathways of a tetrameric beta-sheet complex: molecular dynamics simulations on simplified off-lattice protein models, Biophys. J. 86 (2004) 31–49.
[27] L. Zhang, G.F. Zhao, Y. Sun, Effects of ligand density on hydrophobic charge induction chromatography: molecular dynamics simulation, J. Phys. Chem. B 114 (2010) 2203–2211.
[28] H.J. Berendsen, D. Vanderspoel, R. Vandrunen, Gromacs—a message-passing parallel molecular-dynamics implementation, Comput. Phys. Commun. 91 (1995) 43–56.
[29] E. Lindahl, B. Hess, S.D. van, GROMACS 3.0: a package for molecular simulation and trajectory analysis, J. Mol. Model. 7 (2001) 306–317.
[30] R. Sayle, E. Milnerwhite, RASMOL—biomolecular graphics for all, Trends Biochem. Sci. 20 (1995) 374–376.
[31] L. Zhang, D.N. Lu, Z. Liu, Dynamic control of protein conformation transition in chromatographic separation based on hydrophobic interactions: molecular dynamics simulation, J. Chromatogr. A 1216 (2009) 2483–2490.
[32] D.N. Lu, Z. Liu, Oscillatory molecular driving force for protein folding at high concentration: a molecular simulation, J. Phys. Chem. B 112 (2008) 2686–2693.